J Electr Eng Technol.2015; 10(2): 688-698
http://dx.doi.org/10.5370/JEET.2015.10.2.688

ISSN(Print) 1975-0102
ISSN(Online) 2093-7423

Power Quality Control of Hybrid Wind Power Systems using Robust Tracking Controller

Heesang Ko*, Su-Hyung Yang, Young Il Lee***, Chang-Jin Boo§, Kwang Y. Lee§§ and Ho-Chan Kim†**

Abstract – This paper presents a modeling and a controller design for a hybrid wind turbine generator, especially with an operating mode of battery energy-storage system and a dumpload that contribute to the frequency control of the system while diesel-synchronous unit is not in operation. The proposed control scheme is based on a robust tracking controller, which takes an account of system uncertainties due to the wind flow and load variations. In order to provide robustness for system uncertainties, the range of operation is partitioned into three operating conditions as sub-models in the controller design. In the simulation study, the proposed robust tracking controller (RTC) is compared with the conventional proportional-integral (PI) controller. Simulation results show that the effectiveness of the RTC against disturbances caused by wind speed and load variation. Thus, better quality of the hybrid wind power system is achieved.

Keywords: Hybrid wind power system, Power quality control, Frequency control, Battery energy-storage system, Dumpload, Robust tracking control.

1. Introduction

In remote areas such as small islands, diesel generators are the main source of power supply. Diesel fuel has several drawbacks: it is expensive because transportation to remote areas adds extra cost, and causes air pollution by engine exhaust. Providing a feasible economical and environmental solution to diesel generators is important. A hybrid system of wind power and diesel generators can benefit islands or other isolated communities and increase fuel savings. Wind is, however, a natural energy source that produces a fluctuating power output. The excessive fluctuation of power output adversely affects the quality of power in the distribution system, particularly frequency and voltage [1, 2].

A hybrid generation system is typically composed of a wind turbine coupled with an induction generator, a diesel-synchronous generator unit, a dumpload, and an energy storage system. In the operating with diesel-synchronous generator unit, the system voltage and frequency are controlled well by excitation and governor systems of the synchronous generator. However, it is problematic for frequency control when diesel-synchronous unit is not in operation since load perturbation in a completely isolated power system has a considerable effect on the system frequency. The load perturbation must be dealt with carefully in order to maintain frequency within the allowable range.

To overcome such problem, it is necessary to make use of an energy-storage unit with dumpload. The frequency regulation is accomplished by discharging the energy stored in batteries into the power network whenever there is a sudden frequency drop and charging them when the frequency increases sharply. Battery facilities are well suited for this task because it can provide fast active power compensation. Moreover, the dumpload consumes excessive network power when the battery is fully charged.

In this paper, the frequency is controlled by charging / discharging the battery storage system (BSS) and by absorbing the excess active power from the network with the dumpload, while the excitation system in the synchronous generator is used for the voltage control. If the battery storage is fully charged, the excess power must be absorbed by the dumpload. If the battery storage is not fully charged, the excess power will be charged into the battery and also absorbed by the dumpload. In this case, both the dumpload and the battery storage system operate since the battery is subject to the charging speed.

Some publications are concerned with energy storage system and dumpload combined with a wind turbine in remote areas [3-6]. These works do not provide detailed dynamic models of the battery storage system and the dumpload for stability analysis. In this paper, a nonlinear mathematical model of a hybrid wind system is developed

† Corresponding Author: Dept. of Electrical Engineering, Jeju National University, Korea. (hckim@jejunu.ac.kr)
* Wind Energy Laboratory, Korea Institute of Energy Research. (heesangko@kier.re.kr)
** Doarm Engineering Research Institute, Jeju, Korea. (tngude@naver.com)
*** Dept. of Electrical and Information Engineering, Seoul National University of Science and Technology, Korea. (yilee@snut.ac.kr)
§ Dept. of Electrical Energy Engineering, Jeju International University, Jeju, Korea. (boo1004@jeju.ac.kr)
§§ Dept. of Electrical and Computer Engineering, Baylor University, Waco, USA. (Kwang_Y_Lee@baylor.edu)
Received: August 5, 2014; Accepted: November 11, 2014

for simulation purpose and for designing more effective controllers for power quality improvement. The nonlinear model of a hybrid wind system is formulated in the form of linear state space model with system matrices containing state variables. Thus, the use of robust control method for linear systems can be made for the developed model, where the state dependency of the system matrix is considered as the model uncertainty.

Model predictive control (MPC) is a kind of a finite horizon optimal control implemented in the form of a receding horizon control. Since it provides with closed-loop stability and can effectively deal with constraints on the input or state, MPC has received much attention from both academia and industry [7-10]. In this paper, we adopt a simple Robust Tracking Controller (RTC) [10] to obtain a stabilizing tracking controller. The problem of obtaining robustly stabilizing gains of the controller is formulated in the form of linear matrix inequalities (LMI) so that it can be solved efficiently using software tools. The robust gain of RTC can be used to define a feasible and invariant set around a reference state and additional degrees of freedom can be adopted to enhance the performance and to enlarge the stabilizing region following the receding horizon strategy of MPC as it was done in [10]. But it would be complex and requires heavy computational burden.

This paper is organized as follows: the system model is examined in Section 2, with overall dynamic model given in the Appendix. In Section 3, three sub-models and the robust tracking controllers are developed. In Section 4, simulations are conducted, and conclusions are finally drawn in Section 5.

2. System Model

2.1 System configuration

The hybrid wind system consists of the wind turbine having the induction generator (IG), the diesel engine (DE) with synchronous generator (SG), a battery bank connected with a three-phase thyristor-bridge controlled converter, a dumpload, and the load. A three-phase dumpload is used with each phase consisting of seven transistor-controlled resistor banks. When wind generated power is sufficient to serve the load, the DE is disconnected from the SG by electromagnetic clutch, and the synchronous generator acts as a synchronous condenser.

The main purpose of the dumpload and the battery storage system (BSS) is to regulate the system frequency. The SG (with/without diesel) is used for reactive power control that is achieved by the excitation system to regulate voltage. The SG also contributes the reactive power to compensate for the induction generator. A current source converter is used for the BSS because the charging current can be critical to the battery life. A smooth charging can be achieved using a large inductor in the DC bus minimizing

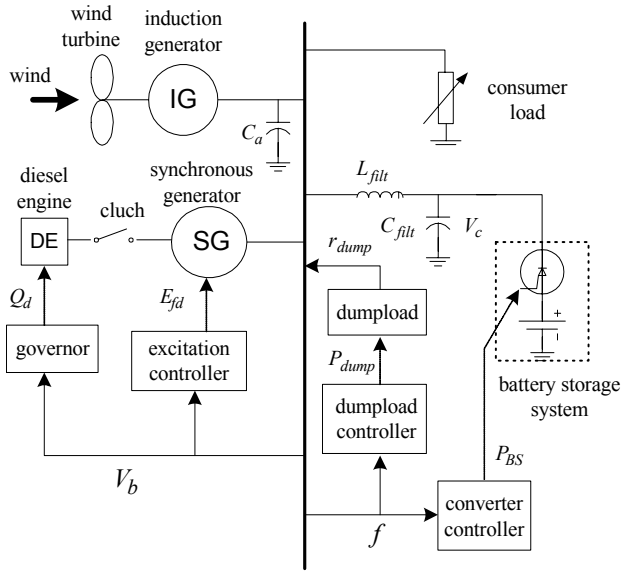

Fig. 1. The overall control action of hybrid wind system

the current fluctuation. Moreover, current source converter is simpler than a voltage source converter.

Fig. 1 shows the overall configuration of the hybrid wind system [11]: C_a is the capacitor bank, Q_d is the fuel flow rate at the governor chamber valve, E_{fd} is the excitation field voltage, f is the frequency, V_b is the bus voltage, L_{filt} is the AC side filter inductance, C_{filt} is the AC side filter capacitance, V_c is the AC side voltage of the converter, and P_{BS} is the battery power. P_{dump} is the dumpload power, and r_{dump} is the dumpload resistance.

2.2 Components models

The models of the generators are based on the standard Park's transformation [12] that transforms all stator variables to the rotor reference frame described by a direct and quadrature (d-q) axis. The set of SG and IG equations are based on the d-q axis in accordance with International Electrotechnical Commission [13].

The nonlinear mathematical model of the hybrid wind system is derived and given in detail in [11] and [14]. The following considerations are taken into account to identify component models: the electrical system is assumed as a perfectly balanced three-phase system with pure sinusoidal voltage and frequency. High frequency transients in stator variables are neglected, which indicates that the stator voltage and currents are allowed to change instantly, because this paper is focused on the transient period instead of sub-transient period. Damper-winding models are ignored because their effect appears mainly in a grid-connected system or a system with several synchronous generators running in parallel. Different component models are of equal level of complexity.

The wind turbine operates in parallel with the battery storage system (BSS) through the current source converter, with or without the controllable dumpload. In either mode

of operation, the diesel engine is disengaged by the clutch, and the synchronous generator is used for the voltage control. The active power is controlled either by the converter or the dumpload. In this section, the reduced-order model for the BSS and the dumpload along with the wind turbine is presented.

The algebraic electrical system equation from Appendix is as follows:

$$\Lambda_{sys}\mathbf{V}_{sys} = \mathbf{E}_{sys} \tag{1}$$

where

$$\mathbf{E_{sys}} = \left[\frac{I_{cq}}{\omega_s^2 C_f L_f - 1} \quad \frac{I_{cd}}{\omega_s^2 C_f L_f - 1} \quad \frac{\omega_s L_{md}}{L_f}\psi_f \; 0 \; 0 \; 0 \; \frac{\omega_s L_m}{L_r}\psi_{rd} \quad -\frac{\omega_s L_m}{L_r}\psi_{rq} \; 0 \; 0 \right]^T$$

and electrical variables are:

$$\mathbf{V_{sys}} = \left[V_{bq} \quad V_{bd} \quad I_{sq} \quad I_{sd} \quad V_{sq} \quad V_{sd} \quad I_{aq} \quad I_{ad} \quad V_{aq} \quad V_{ad} \right]^T \tag{2}$$

The 10×10 electrical system matrix $\mathbf{\Lambda_{sys}}$ is defined in Appendix. The electrical variables in $\mathbf{V_{sys}}$ represent inputs to the 9th-order dynamic model that combines the wind-battery storage system with the dumpload system.

3. Robust Tracking Controller Design

3.1 Control structure

Fig. 2 depicts the input and output relationship of the hybrid wind system from the control point of view. The control inputs are the excitation field voltage (u_1) of the SG, the fuel flow rate at the governor chamber valve (u_2), the battery power (u_3), and the dumpload power (u_4). The measurements are the voltage amplitude (y_1) and the frequency (y_2) of the AC bus. The wind speed (v_1) and the load (v_2) are considered as disturbances. From the control

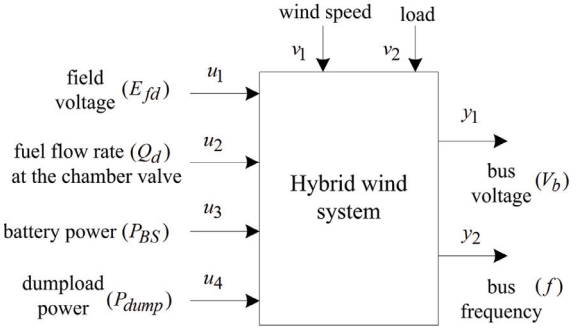

Fig. 2. The structure of the hybrid wind control system

point of view, this model is a coupled 4×2 multi-input-multi-output nonlinear system, since every input controls more than one output and every output is controlled by more than one input.

3.2 Reduced-order model

Since the nonlinear model presented in [11] is too complex to design controllers, there is a need for a reduced-order model that is derived based on practical reasons; i.e., what is measurable and what can be manipulated. With the considerations in section 2.2, the reduced-order model assumes that the dynamic response of the converter is much faster than the desired bandwidth of the controlled system. This implies that the differential equations of the converter are neglected. Also, there is no elasticity in the drive train. Electrical dynamics of the induction generator is not explicitly modeled.

In deriving the nonlinear reduced-order models for the wind-BSS-dumpload system, the same simplifications applied to the previous section are used. In addition, it assumes that the dynamic response of the converter is much faster than the desired bandwidth of the controlled system, which implies that the differential equations of the converter are neglected. Then, the reduced-order model can be represented by the field flux linkage and the angular speed of the SG:

$$\begin{aligned} \dot{\psi}_f &= \frac{1}{\tau_{do}^{'}}\left(-\frac{L_f}{\omega_s L_{md}}(V_{sq} + R_a I_{sq} - \omega_s L_d^{'} I_{sd}) + L_{md} I_{sd} \right) + E_{fd} \\ \dot{\omega}_s &= \frac{1}{J_s}(-T_s) \end{aligned} \tag{3}$$

The control inputs are the field voltage (E_{fd}) and either the dumpload power (P_{dump}) and the battery power (PBS). The outputs are the voltage (V_b) and the frequency ($f=\omega_s$). Eq. (3) needs a modification because the second control input does not explicitly appear in this equation.

The air gap torque of the synchronous generator T_s can be represented as

$$T_s = \frac{P_s}{\omega_s} = \frac{P_{BS} + P_{dump} + P_{load} - P_{ind}}{\omega_s} \tag{4}$$

where P_{BS}, P_{dump}, P_s, and P_{ind} are the power of the battery, the dumpload, the synchronous generator, and the induction generator, respectively.

The reduced-order model becomes

$$\begin{aligned} \dot{\omega}_s &= \frac{1}{J_s}\left(\frac{P_{ind} - P_{load}}{\omega_s} - \frac{1}{\omega_s}P_{BS} - \frac{1}{\omega_s}P_{dump} \right) \\ \dot{\psi}_f &= \frac{1}{\tau_{do}^{'}}\left(-\frac{L_f}{\omega_s L_{md}}(V_{sq} + R_a I_{sq} - \omega_s L_d^{'} I_{sd}) + L_{md} I_{sd} \right) + E_{fd} \end{aligned} \tag{5}$$

With the same procedure as previous section, the final nonlinear reduced-order model is derived in the state-space form as

$$\begin{aligned}\dot{\mathbf{x}}(\mathbf{t}) &= \mathbf{A}_c\mathbf{x}(\mathbf{t}) + \mathbf{B}_c\mathbf{u}(\mathbf{t}) \\ \mathbf{y}(\mathbf{t}) &= \mathbf{C}_c\mathbf{x}(\mathbf{t})\end{aligned} \tag{6}$$

where

$$\mathbf{x}(\mathbf{t}) = \begin{bmatrix} V_b & \omega_s \end{bmatrix}^T, \quad \mathbf{u}(\mathbf{t}) = \begin{bmatrix} E_{fd} & P_{BS} & P_{dump} \end{bmatrix}^T$$

$$\mathbf{A}_c = \begin{bmatrix} -\dfrac{L_f V_{sq}}{\tau_{do}' L_{md} V_b} + \dfrac{(P_{ind} - P_{load})}{J_s \omega_s^2} & \dfrac{L_f}{\tau_{do}' L_{md}}\left(L_d I_{sd} - \dfrac{R_a I_{sq}}{\omega_s}\right) \\ \dfrac{P_{ind} - P_{load}}{J_s V_b \omega_s} & 0 \end{bmatrix}, \tag{7}$$

$$\mathbf{B}_c = \begin{bmatrix} \omega_s & -\dfrac{V_b}{J_s \omega_s^2} & -\dfrac{V_b}{J_s \omega_s^2} \\ 0 & -\dfrac{1}{J_s \omega_s} & -\dfrac{1}{J_s \omega_s} \end{bmatrix}, \quad \mathbf{C}_c = \begin{bmatrix} 1 & 0 \\ 0 & 1 \end{bmatrix}$$

Note that the reduced-order model (6) is in the linear form for fixed system matrices A_c, B_c and C_c. However, matrices A_c and B_c are not fixed, but change as functions of state variables, thus making the model nonlinear. It should be advised that the reduced-order model is only the purpose of the designing controller, not for overall simulation study. The overall simulation is based on the model given in Appendix.

The RTC model represents a nonlinear system by partitioning the system into sub-systems. Three linear sub-systems are considered for the nonlinear state-space model in (6) as

$$\begin{aligned}\dot{x}(t) &= A_{ci}x(t) + B_{ci}u(t) \\ y(t) &= C_{ci}x(t), \quad i = 1, 2, 3\end{aligned} \tag{8}$$

where $A_{ci} \in \Re^{2\times 2}$, $B_{ci} \in \Re^{2\times 3}$, and $C_{ci} \in \Re^{2\times 2}$.

Here, the sub-systems are obtained by partitioning the state-space into three ranges of low, medium, and high levels for output variables V_b and ω_s according to load variations. For each sub-space, different model (i=1, 2, 3) for possible low, the most possible, and possible high cases is applied according to the frequency (ω_s) and voltage (V_b) variation. The continuous-time model (6) can be discretized with sampling period h as

$$\begin{aligned}x[k+1] &= \tilde{A}x[k] + \tilde{B}u[k] \\ y[k] &= Cx[k]\end{aligned} \tag{9}$$

where $x[k] \in \Re^2$, $u[k] \in \Re^3$, and $y[k] \in \Re^2$ are the states, inputs, and outputs, respectively, and the matrices $\tilde{A}$, $\tilde{B}$ and C are obtained as follows

$$\tilde{A} = e^{A_c h}, \quad \tilde{B} = \int_0^h e^{A_c t} B_c dt, \quad C = C_c$$

The objective of the control design is to regulate the output $y[k]$ to the reference signal (thereby $y[k] \to r$). Considering the fact that A_c and B_c change as functions of state variables, we will assume that the system matrices $\tilde{A}$ and $\tilde{B}$ of (9) belong to the following polytopic uncertainty set:

$$\Omega = \left\{ (\tilde{A}, \tilde{B}) = \sum_{i=1}^{n_p} \eta_i (A_i, B_i) \,\middle|\, \eta_i \geq 0, \ \sum_{i=1}^{n_p} \eta_i = 1 \right\} \tag{10}$$

where $A_i = e^{A_{ci} h}$ and $B_i = \int_0^h e^{A_{ci} t} B_{ci} dt$.

This kind of polyhedral type uncertainties are considered in the works of [15-17].

3.3 Robust tracking controller

In this paper, a robust control law is adopted for the discrete-time model (9) and (10) [10]:

Consider the control law

$$\begin{cases} \hat{u}[k] = \hat{u}[k-1] + y[k-1] - r \\ u[k] = Kx[k] + L\hat{u}[k] \end{cases} \tag{11}$$

Note $\hat{u}[k]$ of (11) is the integration of the tracking error, $y(k) - r$. Thus, the proposed control will remove the steady-state error for a constant r if it stabilizes the closed-loop system. In this paper, we will provide a method to determine the gains K and L such that the closed-loop system becomes stable in the presence of the uncertainty described as Ω. Here we consider a constant reference value r and its corresponding reference state x_0 and reference control u_0 satisfying the following relations:

$$\begin{aligned}x_0 &= \tilde{A}x_0 + \tilde{B}u_0 \\ r &= Cx_0\end{aligned} \tag{12}$$

Then, subtracting (12) from (9) yields the error dynamics:

$$e_x[k+1] = \tilde{A}e_x[k] + \tilde{B}e_u[k] \tag{13}$$

where $e_x[k] := x[k] - x_0$ and $e_u[k] := u[k] - u_0$.

Another error dynamics can be obtained as follows by subtracting the steady state value of $\hat{u}(k)$ from the both sides of the first equation of (11):

$$\hat{e}_u[k] = \hat{e}_u[k-1] + Ce_x[k-1] \tag{14}$$

where $\hat{e}_u[k] := \hat{u}[k] - \hat{u}[\infty]$. Combining (13) and (14), we

have:

$$\begin{aligned} \tilde{e}[k+1] &= \tilde{A}_t \tilde{e}[k] + \tilde{B}_t e_u[k] \\ e_u[k] &= F_t \tilde{e}[k] \end{aligned} \quad (15)$$

where $\tilde{e}[k] = \begin{bmatrix} e_x[k] \\ \hat{e}_u[k] \end{bmatrix}$ and $F_t = \begin{bmatrix} K & L \end{bmatrix}$, $\tilde{A}_t = \begin{bmatrix} \tilde{A} & 0 \\ C & I_2 \end{bmatrix}$, $\tilde{B}_t = \begin{bmatrix} \tilde{B} \\ 0 \end{bmatrix}$.

Then, (15) can be rewritten as:

$$\tilde{e}[k+1] = (\tilde{A}_t + \tilde{B}_t \tilde{F})\tilde{e}[k] \quad (16)$$

and the problem of finding stabilizing gain $\tilde{F} = [K \; L]$ boils down to a standard state-feedback stabilization problem. Therefore, the gains stabilizing (16) can be obtained using the well known feedback design methods [15] as follows.

Consider a Lyapunov candidate function

$$V[k] = \tilde{e}[k]^T Q \tilde{e}[k] \; (Q > 0) \quad (17)$$

Then, it is easy to see that $V[k] > V[k+1]$ is guaranteed if

$$(\tilde{A}_t + \tilde{B}_t \tilde{F})^T Q (\tilde{A}_t + \tilde{B}_t \tilde{F}) - Q < 0 \quad (18)$$

is met for all possible values of $\tilde{A}_t$ and $\tilde{B}_t$. Using the Schur-complement [18], (18) can be transformed into the following LMI:

$$\begin{bmatrix} R & \left(\tilde{A}_t R + \tilde{B}_t Y\right)^T \\ \tilde{A}_t R + \tilde{B}_t Y & R \end{bmatrix} > 0 \quad (19)$$

where $R = Q^{-1}$ and $Y = \tilde{F}R$. Since the matrix set (A, B) belongs to the uncertainty set Ω of (10), (19) can be guaranteed if it is met at every corners of Ω. Thus, the origin of the closed-loop system (16) is asymptotically stable in the presence of the uncertainty Ω if there exist a matrices $R = Q^{-1} > 0$ and Y such that

$$\begin{bmatrix} R & \left(\tilde{A}_{t,i} R + \tilde{B}_{t,i} Y\right)^T \\ \tilde{A}_{t,i} R + \tilde{B}_{t,i} Y & R \end{bmatrix} > 0, \text{ for } i = 1,2,3, \quad (20)$$

where $\tilde{A}_{t,i} = \begin{bmatrix} A_i & 0 \\ C & I_2 \end{bmatrix}$, $\tilde{B}_{t,i} = \begin{bmatrix} B_i \\ 0 \end{bmatrix}$ and the feedback gains are determined as $\tilde{F} = YR^{-1}$. The choice of R and Y satisfying the LMI (20), however, is not unique and we have to define an optimization problem to select one set of matrices R and Y. In order to make $V[k]$ decreases as soon as possible in the presence of uncertainties, we can define an optimization problem as follows

$$\min_{R,Y} \; \lambda(R) \quad \text{subject to (20)} \quad (21)$$

and

$$R > \alpha I \quad (22)$$

where $\lambda(R)$ is the generalized eigenvalue of R. Note that to control gain F_t becomes large when R becomes small and the additional constraint (22) is used to constrain the magnitude of control gains. The problem (21) can be solved effectively using a semi-definite programming. Note that the control (14) can be modified to yield the incremental formulation by subtracting $u[k-1]$ from $u[k]$ as follows:

$$u[k] = u[k-1] + K\left(x[k] - x[k-1]\right) + L\left(y[k-1] - r\right) \quad (23)$$

This formulation helps to obtain a bumpless switching between manual or open-loop mode to closed-loop mode.

4. Evaluation by Simulation

4.1 System parameters

The system under study consists of a horizontal axis, 3-bladed, stall regulated wind turbine with a rotor of 16.6 m diameter, that runs an induction generator (IG) rated at 55 kW. The IG is connected to an AC bus in parallel with a diesel-synchronous generator unit that consists of a 50 kW turbocharged diesel engine (DE) driving a 55 kVA brushless synchronous generator (SG). Nominal system frequency is 50 Hz, and the rated line AC voltage is 230 V [19]. The battery storage is connected to the AC bus through a thyristor-bridge controlled current source converter rated at 55 kW. A load is rated at 40 kW. The inertia of the IG is 1.40 kgm^2, and the inertia of the SG is 1.11 kgm^2. The three-phase dumpload is used where each phase consists of 7 transistor-controlled resistor banks with binary resistor sizing in order to minimize quantum effects and provide near linear esolution.

The controller design parameters for the PI controllers of the governor, the excitation system, the converter, and the dumpload are set with the proportional gain 30 and the integral gain 90. The time-step size for overall simulation is 1ms.

Three linear models for possible low, the most possible, and possible high cases are obtained from (8) applying L=0.9 p.u., M=1.0 p.u., and H=1.1 p.u. for both V_b and f.

$$A_{C1}=\begin{bmatrix}-0.1978 & -0.6759\\ 1.7527 & 0\end{bmatrix},\ B_{C1}=\begin{bmatrix}0.5 & -4.0163 & -4.0163\\ 0 & -4.0163 & -4.0163\end{bmatrix}$$
$$A_{C2}=\begin{bmatrix}-0.5371 & -0.6763\\ 0.4382 & 0\end{bmatrix},\ B_{C2}=\begin{bmatrix}1 & -2.0082 & -2.0082\\ 0 & -2.0082 & -2.0082\end{bmatrix}$$
$$A_{C3}=\begin{bmatrix}-0.4554 & -0.6765\\ 0.1947 & 0\end{bmatrix},\ B_{C3}=\begin{bmatrix}1.5 & -1.3388 & -1.3388\\ 0 & -1.3388 & -1.3388\end{bmatrix} \quad (24)$$

The control gain K and L were determined by solving the (18) and (20):

$$K=\begin{bmatrix}-1334.0 & 1334.6\\ 9.9 & 122.5\\ 32.4 & 125.7\end{bmatrix},\ L=\begin{bmatrix}-333.9 & 333.7\\ -0.02 & 16.3\\ 6.3 & 19.1\end{bmatrix} \quad (25)$$

4.2 Hybrid wind power system control

This simulation is to examine how the battery storage system (BSS) and the dumpload work for better frequency control, and how they contribute the voltage control with the excitation system in the SG. Fig. 3 shows the wind speed, which can be described by a Weibull probability distribution. While the DG is shutdown, the load is changed from 38 kW to 20 kW at 5 sec. During the transient period from 5 sec. to 6 sec., the battery bank is charged with the speed of 700 W/sec. In the steady state, the battery is charged in 2 W/sec. Fig. 4 and Fig. 5 show the comparison of the active power of the IG, load, the dumpload, and the battery storage. It is observed that the proposed RTC has much faster response to the disturbance compared to the PI control.

Fig. 6 and Fig. 7 show the comparison of the responses of the frequency and the voltage. Compared to the PI control, the frequency response of the RTC is excellent except for a slight bias from the nominal frequency, while the voltage response is sluggish compared to the PI control. From the simulation study, the proposed controller achieves

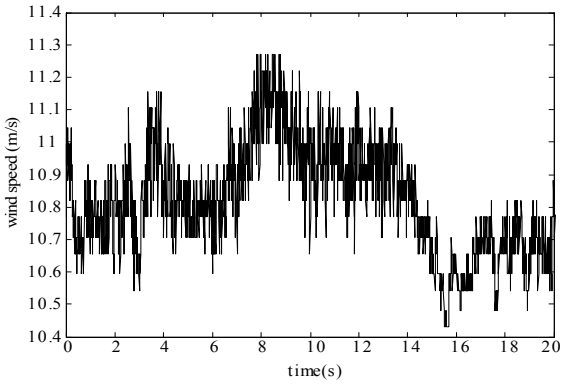

Fig. 3. Wind speed in the charge operation

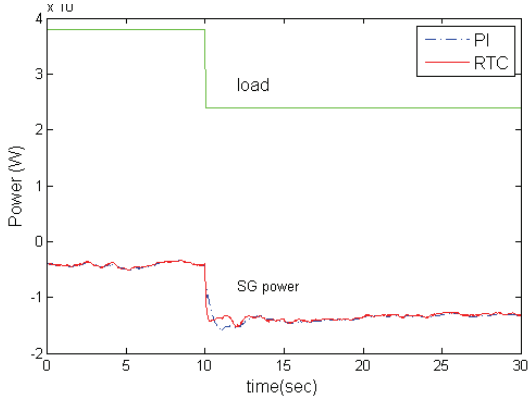

Fig. 4. Load change and power output of the SG

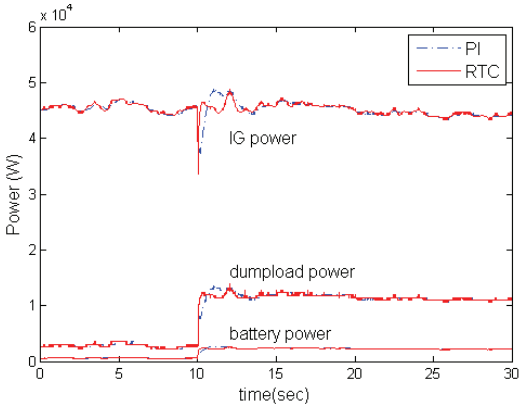

Fig. 5. Power outputs of the IG, the dumpload, and the battery storage

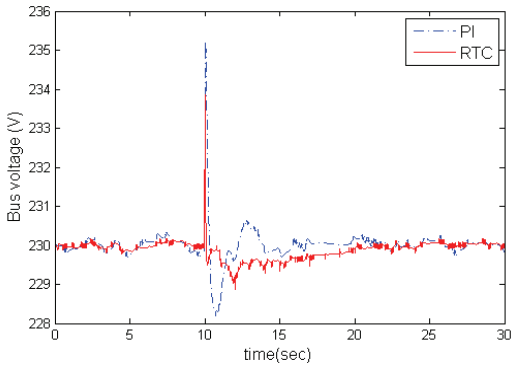

Fig. 6. Bus voltage

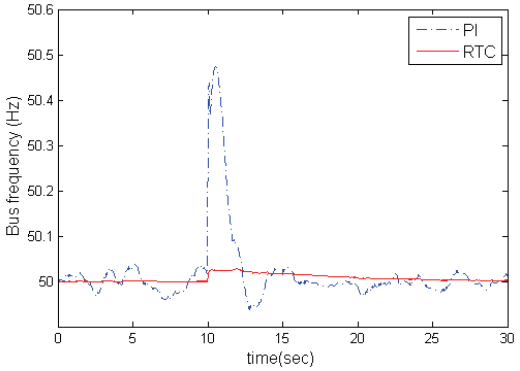

Fig. 7. Bus fr equency

the smoother and tighter power quality control in terms of the frequency, wind generator power, diesel generator power, battery power and dumpload.

The sluggish response of the voltage suggests that there is a room for further improvement in the robust tracking control. For a future work, a robust tracking model predictive control (MPC) is planned to enhance the robust performance in the presence of uncertainties of the reduced and discretized model as well as the uncertainties of the wind speed.

5. Conclusion

In this paper, the robust tracking controller is presented for the study of the power quality of the hybrid wind power system. The derived simulation model including the reduced-order model can be applied for different hybrid wind power system configurations to study power quality control. The proposed control scheme provides more effective control for the system to achieve better power quality, which is demonstrated by smooth transition of frequency, wind turbine generator, diesel generator, battery charge and dumpload. Thus, the usefulness of the robust tracking control is demonstrated in this paper. For a future work, a robust tracking MPC will be designed to enhance the robust performance in the presence of uncertainties of the reduced and discretized model as well as the uncertainties of the wind speed. The key issue of the future work will be to reduce the computational burden.

Appendix

The overall dynamic model representing of Fig. 1 is as follows:

The aerodynamic power is given by

$$P_w = \frac{1}{2} C_p(\lambda,\zeta)\rho A_r V_w^3$$

where

$C_p(\lambda,\zeta)$: total power coefficient

λ : tip speed ratio, $\lambda = \lambda_0 + 0.08\zeta$ and $\left(\lambda_0 = \frac{\omega_t r}{V_w}\right)$

ζ : pitch angle

ρ : air density [Kg/m^2]

A_r : swept area of the rotor [m^2]

V_w : wind speed [m/s] and $C_p(\lambda,\zeta)$ parameters

λ	1	2	3	4	5	6
C_p	0	0.0607	0.1989	0.3283	0.4214	0.4508
λ	7	8	9	10	11	
C_p	0.4067	0.2891	0.1323	0.025	0	

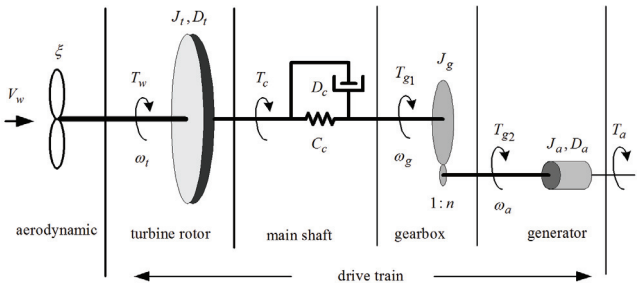

Fig. 8. A simplified block diagram of the wind turbine

The algebraic electrical system equation to represent of the network is as follows:

$$\Lambda_{sys}\mathbf{V}_{sys} = \mathbf{E}_{sys} \quad \text{(A1)}$$

where

$$\Lambda_{sys} = \begin{bmatrix} \Lambda_1 & \Lambda_2 & \Lambda_3 \\ \Lambda_4 & \Lambda_5 & \Lambda_6 \\ \Lambda_7 & \Lambda_8 & \Lambda_9 \end{bmatrix}$$

$$\mathbf{E_{sys}} = \left[\frac{I_{cq}}{\omega_s^2 C_f L_f - 1} \;\; \frac{I_{cd}}{\omega_s^2 C_f L_f - 1} \;\; \frac{\omega_s L_{md}}{L_f}\psi_f \;\; 0 \;\; 0 \;\; \frac{\omega_s L_m}{L_r}\psi_{rd} \;\; -\frac{\omega_s L_m}{L_r}\psi_{rq} \;\; 0 \;\; 0 \right]^T$$

and electrical variables are:

$$\mathbf{V_{sys}} = \left[V_{bq} \;\; V_{bd} \;\; I_{sq} \;\; I_{sd} \;\; V_{sq} \;\; V_{sd} \;\; I_{aq} \;\; I_{ad} \;\; V_{aq} \;\; V_{ad} \right]^T$$

where

ω_s : bus frequency (or angular speed of SG)

L_r, L_{md} : rotor and *d*-axis mutual inductances of SG

C_f, L_f : field capacitance and inductance of SG

$\psi_f, \psi_{rq}, \psi_{rd}$: filed and rotor flux linkages of SG

V_{bq}, V_{bd} : *q*-axis and *d*-axis bus voltages

$I_{sq}, I_{sd}, V_{sq}, V_{sd}$: current component of SG into the bus and stator terminal voltage components of SG

$I_{aq}, I_{ad}, V_{aq}, V_{ad}$: stator terminal current and voltage of IG

The 10×10 electrical system matrix is:

$$\Lambda_1 = \begin{bmatrix} \frac{R_3}{R_3^2 + X_3^2} + \frac{1}{r_{dump}} & \frac{X_3}{R_3^2 + X_3^2} \\ -\frac{X_3}{R_3^2 + X_3^2} & \frac{R_3}{R_3^2 + X_3^2} + \frac{1}{r_{dump}} \end{bmatrix},$$

$$\Lambda_2 = \begin{bmatrix} -1 & 0 & 0 & 0 \\ 0 & -1 & 0 & 0 \end{bmatrix},$$

$$\Lambda_3=\begin{bmatrix}-1 & 0 & 0 & -\omega_s C_a\\ 0 & -1 & \omega_s C_a & 0\end{bmatrix},\quad \Lambda_4=\Lambda_7=\begin{bmatrix}0 & 0\\ 0 & 0\\ 1 & 0\\ 0 & 1\end{bmatrix},$$

$$\Lambda_5=\begin{bmatrix}R_a & -\omega_s L_d^{'} & 1 & 0\\ \omega_s L_q & R_a & 0 & 1\\ R_1 & -\omega_s L_1 & -1 & 0\\ \omega_s L_1 & R_1 & 0 & -1\end{bmatrix},\ \Lambda_6=\Lambda_8=\begin{bmatrix}0 & 0 & 0 & 0\\ 0 & 0 & 0 & 0\\ 0 & 0 & 0 & 0\\ 0 & 0 & 0 & 0\end{bmatrix},$$

$$\Lambda_9=\begin{bmatrix}R_s & -\omega_s L_s^{'} & 1 & 0\\ \omega_s L_s^{'} & R_s & 0 & 1\\ R_2 & -\omega_s L_2 & \omega_s^2 L_2 C_a-1 & \omega_s R_2 C_a\\ \omega_s L_2 & R_2 & -\omega_s R_2 C_a & \omega_s^2 L_2 C_a-1\end{bmatrix}$$

where

R_3, X_3 : equivalent load resistance and reactance
R_1, L_1 : resistance and reactance between SG and bus
R_2, L_2 : resistance and reactance between IG and bus
$R_a, L_d^{'}$: rotor resistance and *d*-axis inductance of SG
C_a : capacitor bank of wind turbine
$R_s, L_s^{'}$: stator resistance and inductance of SG

The electrical variables in $\mathbf{V_{sys}}$ represent inputs to the 10[th]-order dynamic system that complete the wind-diesel system model.

The modeling of the SG and the IG generator is based on [11].

Diesel-synchronous generator (salient pole):

$$\begin{aligned}
\dot{Q}_f &= \frac{1}{\tau_c}\left(-Q_f + Q_d(t-\tau_d)\right)\\
\dot{\theta}_{cl} &= \omega_d - \omega_s\\
\dot{\omega}_d &= \frac{1}{J_d}\left(k_c k_v Q_f - (D_d + D_{cl})\omega_d + D_{cl}\omega_s - k_v p_o - C_{cl}\theta_{cl}\right)\\
\dot{\psi}_f &= \frac{1}{\tau_{do}^{'}}\left(-\psi_f + L_{md} I_{sd}\right) + E_{fd}\\
\dot{\omega}_s &= \frac{1}{J_s}\left(C_{cl}\theta_{cl} + D_{cl}\omega_d - T_s - (D_{cl} + D_s)\omega_s\right)\\
\dot{\psi}_f &= \frac{1}{\tau_{do}^{'}}\left(-\psi_f + L_{md} I_{sd}\right) + E_{fd}\\
\dot{\omega}_s &= \frac{1}{J_s}\left(C_{cl}\theta_{cl} + D_{cl}\omega_d - T_s - (D_{cl} + D_s)\omega_s\right)
\end{aligned} \tag{A2}$$

where $T_s = -\frac{L_{md}}{L_f}\psi_f I_{sq} - (L_d^{'} - L_q) I_{sq} I_{sd}$ and

E_{fd} : filed flux linkage of SG
J_s, D_s : inertia and frictional damping of SG
T_s : air gap torque of SG
$\tau_{do}^{'}$: transient open circuit time constant
Q_f : fuel flow rate into the combustion chamber
Q_d : fuel flow rate at the governor chamber valve
p_o : zero torque pressure when running idle
τ_d : time delay of combustion
k_v : stroke volume of the engine
k_c : a constant describing efficiency of combustion
θ_{cl} : torsional angle between the engine and the generator shaft

Induction generator (squirrel-cage rotor):

$$\begin{aligned}
\dot{\psi}_{rq} &= \frac{1}{\tau_o^{'}}(-\psi_{rq} + L_m I_{aq}) + \omega_b(\omega_s - \omega_a)\psi_{rd}\\
\dot{\psi}_{rd} &= \frac{1}{\tau_o^{'}}(-\psi_{rd} + L_m I_{ad}) - \omega_b(\omega_s - \omega_a)\psi_{rq}
\end{aligned} \tag{A3}$$

where

ω_a : angular speed of wind turbine
$\tau_o^{'}$: transient open circuit time constant
L_m : mutual inductance of SG

Drive train model (shaft between rotor turbine and the IG):

$$\begin{aligned}
\dot{\theta}_c &= \omega_t - \omega_a\\
\dot{\omega}_t &= \frac{1}{J_t}\left(\frac{P_w}{\omega_t} - C_c\theta_c - (D_t + D_c)\omega_t + D_c\omega_a\right)\\
\dot{\omega}_a &= \frac{1}{J_a}\left(C_c\theta_c + D_c\omega_t - (D_a + D_c)\omega_a - T_a\right)
\end{aligned} \tag{A4}$$

where

ω_t : bus frequency (or angular speed of IG)
T_a : air gap torque of IG

Current balance form for electrical model:

$$I_{sq} + I_{iq} - I_{lq} - I_{ac,q} = 0,\quad I_{sd} + I_{id} - I_{ld} - I_{ac,d} = 0 \tag{A5}$$

where current component of the load (I_{lq}, I_{ld}) and current component of IG into the bus (I_{iq}, I_{id}) are given

$$\begin{aligned}
I_{lq} &= \left(\frac{R_3}{R_3^2 + X_3^2} + \frac{1}{r_{dump}}\right)V_{bq} + \frac{X_3}{R_3^2 + X_3^2}V_{bd},\\
I_{ld} &= -\frac{X_3}{R_3^2 + X_3^2}V_{bq} + \left(\frac{R_3}{R_3^2 + X_3^2} + \frac{1}{r_{dump}}\right)V_{bd},
\end{aligned} \tag{A6}$$

where R_3, X_3 is equivalent load resistance and reactance, and

$$\begin{aligned}
I_{iq} &= I_{aq} + \omega_s C_a V_{ad}, \qquad I_{id} = I_{ad} - \omega_s C_a V_{aq},\\
I_{ac,q} &= \frac{-\omega_s C_{filt}}{1 - \omega_s^2 C_{filt} L_{filt}}V_{cd} + \frac{1}{1 - \omega_s^2 C_{filt} L_{filt}}I_{cq},\\
I_{ac,d} &= \frac{\omega_s C_{filt}}{1 - \omega_s^2 C_{filt} L_{filt}}V_{cq} + \frac{1}{1 - \omega_s^2 C_{filt} L_{filt}}I_{cd}
\end{aligned} \tag{A7}$$

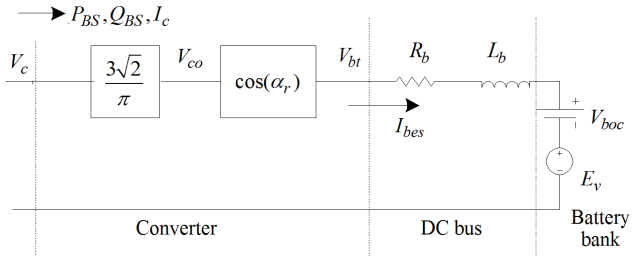

Fig. 9. Equivalent circuit of the battery storage system in the rectifier operation

where

$I_{cq}, I_{cd}, V_{cq}, V_{cd}$: AC side current and voltage of the converter

$I_{ac,q}, I_{ac,d}$: AC side current before the filters

The energy storage system is consisted of power converter and battery bank [20]. The power converter for controlling of charging and discharging of battery can be represented for the simulation purpose as shown in Fig. 9 [21].

Here, the firing angle (α_r) is controlled by the internal PI controller. $u_c(=\pi/2-\alpha_r)$ is the output of the PI converter controller, K_P is the proportional gain and K_I is the integral gain. To represent the charging speed of the BSS, the forcing voltage (E_v=$K_{v,ref}I_{bes}$) is made dependent to the DC current (I_{bes}) in DC bus where $K_{v,ref}$ is the forcing gain. The battery is represented as follows:

$$\begin{aligned} \dot{I}_{bes} &= \frac{1}{L_b}[V_{bt} - R_b I_{bes} - V_{boc} - E_v] \\ \dot{x}_{PI} &= \frac{1}{K_I}(I_{ref} - I_{bes}) \\ u_c &= x_{PI} + K_P(I_{ref} - I_{bes}) \end{aligned} \tag{A8}$$

where

R_b, L_b : total resistance (battery internal + DC line) and DC line inductance

V_{boc}, I_{ref} : open circuit DC voltage and current setpoint for the converter

By connecting the battery storage to the AC bus, the charging and discharging power P_{BS}, Q_{BS} can be described as

$$\begin{aligned} P_{BS} &= V_{cd}I_{cd} + V_{cq}I_{cq}, \\ Q_{BS} &= V_{cd}I_{cq} - V_{cq}I_{cd} \end{aligned} \tag{A9}$$

Therefore, the equivalent converter currents I_{cd} and I_{cq} can be obtained. Here, $P_{c,loss}$ is the constant power loss in the thyristor. The currents for current balance form can be obtained as follows:

Table 1. Per-unit base values.

Terms	Symbols	Parameters
Angular speed	ω_b	2π50 rad/sec
Power	S_b=P_b=Q_b	55000 VA
Line AC voltage	V_b	230 V(rms)
DC voltage	V_{dc}	230 V
AC current	$I_b = S_b/\sqrt{3}V_b$	138 A
DC current	$I_{dc} = S_b/V_{dc}$	239 A
Resistance	$R_{base} = V_b^2/S_b$	0.96 Ω
Inductance	$L_{base} = R_{base}/\omega_b$	3.06 mH
Capacitance	$C_{base} = 1/(R_{base}\omega_b)$	3.31 mF
Torque	$T_b = S_b/\omega_b$	175.1 Nm
Moment of inertia	$J_{base} = S_b/\omega_b^2$	0.557 kgm^2/s
Torsional stiffness	$C_{T,base} = T_{base}/rad$	175.1 Nm/rad
Torsional damping	$D_{T,base} = T_{base}/\omega_b$	0.557 Nms/rad

$$\begin{aligned} I_{cq} &= \frac{V_{cq}P_{BS} + V_{cd}Q_{BS}}{V_c^2}, \\ I_{cd} &= \frac{V_{cd}P_{BS} - V_{cq}Q_{BS}}{V_c^2} \end{aligned} \tag{A10}$$

The per-unit system is used in modeling the wind-diesel mechanical and electrical system, where the base values are given below:

Acknowledgements

This work was supported in part by Basic Science Research Program through the National Research Foundation of Korea (NRF) funded by the Ministry of Education, Science and Technology (2011-0012202), and in part by the Research and Development Program of the Korea Institute of Energy Research (KIER) (B4-2453-01).

References

[1] L.L. Feris, *Wind Energy Conversion System*, New Jersy: Prentice Hall, 1990.

[2] R. Hunter and G. Elliot, *Wind-Diesel Systems*, New York: Cambridge University, 1994.

[3] G. Notton, C. Cristofari, P. Poggi, and M. Muselli, "Wind hybrid electrical supply system: behavior simulation and sizing optimization," *Wind Energy*, vol. 4, pp. 43-59, 2001.

[4] M.D. Mufti, R. Balasubramanian, and S.C. Tripathy, "Dynamic performance assessment of an isolated wind-diesel power system with superconducting magnetic energy storage unit under turbulent wind and load disturbances," *International Journal of*

Energy Research, vol. 26, pp. 185-201, 2002.
[5] M.H. Nehrir, B.J. Lameres, G. Venkataramanan, V. Gerez, and L.A. Alvarado, "An approach to evaluate the general performance of stand-alone wind / photovoltaic generating systems," *IEEE Transactions on Energy Conversion*, vol.15, pp.433-439, 2000.
[6] J.T. Bialasiewicz, E. Muljadi, S. Drouilhet, and G. Nix, "Hybrid power systems with diesel and wind turbine generation," *In Proceeding of American Control Conference*, vol. 3, pp. 1705-1709, Philadelphia, USA, 1998.
[7] M. Morari and J. Lee, "Model predictive control – past, present and future," *Computers and Chemical Engineering*, vol. 23, pp. 667-682, 1999.
[8] D.Q. Mayne, J.B. Rawlings, C.V. Rao, and P.O.N. Scokaert, "Constrained model predictive control: Stability and optimality," *Automatica*, vol. 36, pp. 789-814, 2000.
[9] S.J. Qin and T.A. Badgwell, "A survey of industrial model predictive control technology," *Control Engineering Practice*, vol. 11, pp. 733-964, 2003.
[10] J.S. Lim, J.S. Kim, and Y.I. Lee, "Robust tracking model predictive control for input-constrained uncertain linear time invariant systems," *International Journal of Control*, vol. 87, pp. 120-130, 2014.
[11] H.S. Ko, K.Y. Lee, and H.-C. Kim, "Intelligent controller design for a remote wind-diesel power system: Design and dynamic performance analysis," *Wind Power Systems: Application of Computational Intelligence* (*L. Wang, C. Singh, and A. Kusiak, Editors*), pp. 297-335, 2010.
[12] International Electrotechical Commission, Publication 34-10, *Rotating electrical machines, Part 10: Conventions for description of synchronous machines, Geneve*, 1975.
[13] P.C. Krause, O. Wasynczuk, and S.D. Sudhoff, *Analysis of Electrical Machinery*, New York: McGraw-Hill, 1986.
[14] S.H. Yang, H.C. Kim, C.J. Boo, Y.I. Lee, J.S. Lim, H.S. Ko, and K.Y. Lee, "Power quality control of hybrid wind power systems using robust tracking controller," *In IFAC Symposium on Power Plant & Power Systems*, pp. 1-6, Toulouse, France, 2012 September.
[15] M.V. Kothare, V. Balakrishnan, and M. Morari, "Robust constrained model predictive control using linear matrix inequalities," *Automatica*, vol. 32, no. 10, pp. 1361-1379, 1996.
[16] D.Q. Mayne, M.M Seron, and S.V. Rakovic, "Robust model predictive control of constrained linear systems with bounded disturbances," *Automatica*, vol. 41, no. 2, pp. 219-224, 2005.
[17] J.S. Lim, S.Y. Son, and Y.I. Lee, "Receding horizon output feedback control for constrained uncertain systems using periodic invariance," *International Journal of Control*, vol. 83, no. 6, pp. 1277-1286, 2010.
[18] L, Vandenberghe, S. Boyd, and S.P. Wu, "Determinant Maximization with Linear Matrix Inequality Constraints," *SIAM Journal on matrix analysis and applications*, vol. 19, no. 2, pp. 499-533, 1998.
[19] K. Uhlen, B.A. Foss, and O.B. Gjosaeter, "Robust control and analysis of a wind-diesel hybrid power plant," *IEEE Trans. on Energy Conversion*, vol.9, no. 4, pp. 701-708, 1994.
[20] Hee-Sang Ko, *Microgrid Power System Dynamic Modeling*, Technical Report, Wind Energy Laboratory, Korea Institute of Energy Research, 2013.
[21] J.G. Kassakian, M.F. Schlecht, and G.C. Verghese, *Principles of Power Electronics*, New York: Addison-Wesley Publishing, 1992.

Hee-Sang Ko He received his B.S. degree in Electrical Engineering from Jeju National University, Jeju, Korea, in 1996, his M.Sc. degree in Electrical Engineering from Pennsylvania State University, University Park, USA, in 2000, and his Ph.D. in Electrical and Computer Engineering from the University of British Columbia, Vancouver, Canada, in 2006. He was the project leader in wind turbine business division at Samsung Heavy Industries until 2013. He is currently a Chief in the wind energy laboratory at Korea Institute of Energy Research (KIER), Daejeon, Korea. His research interests include wind power technologies, power system stability, microgrid, control design, and system identification.

Su-Hyung Yang He received his B.S. and M.S degree from Electrical Engineering at Jeju National Univ., Korea in 2010 and 2012, respectively. He is currently working in Doarm Engineering Corporation. His research interest is wind power system.

Young Il Lee He received his B.Sc., M.S. and Ph.D in Control & Instrumentation from Seoul National University in 1986, 1988 and 1993, respectively. He worked at Gyeongsang National University from 1994 to 2001 as an Associate Professor and he is currently with Seoul National University of Science and Technology since 2001 as a Professor. He visited Oxford University as a Visiting Research Fellow for the period of 1998-1999 and 2007. He was editor of international journal of control, automation and systems. His research interests include model predictive control and its application to power converters and electrical machines.

Chang-Jin Boo He received his B.S., M.S., and Ph.D. degrees in Electrical Engineering from Jeju National University in 2001, 2003 and 2007, respectively. Since 2014, he has been with the Department of Electrical Energy Engineering at Jeju International University, where he is currently an Assistant Professor. His research interests include grounding system, smartgrid, and power system control.

Kwang Y. Lee He received his B.S. degree in Electrical Engineering from Seoul National University, Korea, in 1964, M.S. degree in Electrical Engineering from North Dakota State University, Fargo, in 1968, and Ph.D. degree in System Science from Michigan State University, East Lansing, in 1971. He has been with Michigan State, Oregon State, Univ. of Houston, the Pennsylvania State University, and Baylor University where he is currently a Professor and Chair of Electrical and Computer Engineering. His interests include power system control, operation, planning, and intelligent system applications to power systems. Dr. Lee is a Fellow of IEEE, Editor of IEEE Transactions on Energy Conversion, and Former Associate Editor of IEEE Transactions on Neural Networks. He is also a registered Professional Engineer.

Ho-Chan Kim He received the B.S., M.S., and Ph.D. degrees in Control & Instrumentation Engineering from Seoul National University in 1987, 1989, and 1994, respectively. Since 1995, he has been with the Department of Electrical Engineering at Jeju National University, where he is currently a professor. He was a Visiting Scholar at the Pennsylvania State University in 1999 and 2008. His research interests include wind power control, electricity market analysis, and grounding systems.